Engineered Nanostructures for High Thermal Conductivity Substrates

Kripa K.Varanasi[1*], Tao Deng, Pramod Chamarthy, Shakti Chauhan, Peter de Bock, Tao Deng, Ambarish Kulkarni, Gary Mandrusiak, Brian Rush, Boris Russ, Lauraine Denault, Stanton Weaver, Frank Gerner[3], Quinn Leland[4], Kirk Yerkes[4]
[1]Massachusetts Institute of Technology, Cambridge, MA, GE Global Research Center, Niskayuna, NY, [3]University of Cincinnati, Cincinnati, OH, [4]Air Force Research Lab, Dayton, OH

ABSTRACT

In the DARPA Thermal Ground Plane (TGP) program[1],we are developing a new thermal technology that will enable a monumental thermal technological leap to an entirely new class of electronics, particularly electronics for use in high-tech military systems. The proposed TGP is a planar, thermal expansion matched heat spreader that is capable of moving heat from multiple chips to a remote thermal sink. DARPA's final goals require the TGP to have an effective conductivity of 20,000 W/mK, operate at 20g, with minimal fluid loss of less than 0.1%/year and in a large ultra-thin planar package of 10cmx20cm, no thicker than 1mm. The proposed TGP is based on a heat pipe architecture[2], whereby the enhanced transport of heat is made possible by applying nanoengineered surfaces to the evaporator, wick, and condenser surfaces. Ultra-low thermal resistances are engineered using superhydrophilic and superhydrophobic nanostructures on the interior surfaces of the TGP envelope. The final TGP design will be easily integrated into existing printed circuit board manufacturing technology. In this paper, we present the transport design, fabrication and packaging techniques, and finally a novel fluorescence imaging technique to visualize the capillary flow in these nanostructured wicks.

Keywords: heat pipes, wicking, capillarity, fluorescence imaging, superhydrophobic, superhydrophilic surfaces

1 INTRODUCTION

A key challenge in thermal management is the capability to remove heat from the device while maintaining acceptable component operating temperatures. As electronics power densities continue to increase, thermal management of electronics becomes increasingly important. Commonly, it is sought to remove heat with minimal temperature rise, which contributes to a desire for cooling solutions to have minimal thermal resistance.

Common thermal bottlenecks in electronics cooling solutions are the thermal interface, conduction and convection resistances. In order to reduce convection resistances, one can attempt to either increase the convective heat transfer coefficients or increase convective surface area. As it is often challenging to increase heat transfer coefficients due to fluid selection or pumping power limitations, the increase of convective surface area by means of larger or finned surfaces is often pursued. The relative effectiveness of lowering convective thermal resistance by increasing surface area diminishes as at some point conduction (spreading) resistance lowers the effectiveness of additional fin area. In order to address this limitation, several high performance heat sinks have heat pipes embedded in them to facilitate heat transport.

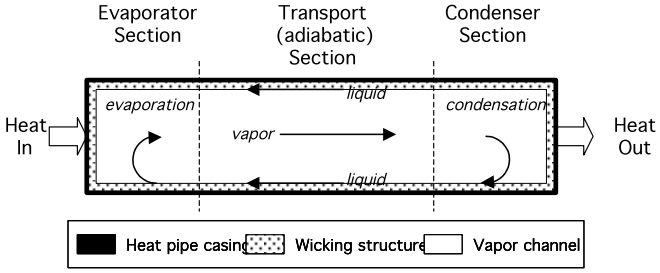

Figure 1: Heat pipe configuration

Heat pipes are devices that aid in the transport of heat by means of two-phase heat transfer. Figure 1 depicts a sketch of a common heat pipe configuration. A heat pipe consists of a hollow casing with an internal wick structure and vapor channel. In the heat pipe, the wick structure is saturated with a working fluid that is in equilibrium with saturated vapor in the vapor channel. The liquid evaporates at the end where heat is added to the system. This evaporation causes an increase in vapor pressure, which drives flow to the condenser region. At the condenser, heat is rejected as vapor condenses to a liquid, which is still at relatively high pressure. This high-pressure liquid is then driven toward the evaporator where the liquid is at a lower pressure. Capillary forces in the wick structure drive this liquid transport. The wick structure is a critical component of the heat pipe both for its mass transport and heat transfer characteristics. Experimental validation of wick characteristics is crucial for the development of high performance heat pipes [3,8]. This study focuses on a method to characterize the capillary performance of wick structures with micro- and nano-sized pores.

2 EXPERIMENTAL METHODS

Several methods have been described in literature to study the capillary performance of wick structures [3,4]. The simplest method is the rising meniscus method [5]. In a possible variant of this method, a section of the wick is submerged in an open reservoir and the rise of liquid in the wick is measured. The height of the liquid column is a metric for the capillary performance of the wick structure.

This height (h) is a function of the equilibrium between the capillary (ΔP_c) and the hydrostatic (ΔP_g)

* Corresponding authors: Prof. Kripa Varanasi, varanasi@mit.edu, Dr. Tao Deng, dengt@research.ge.com

pressures at the liquid interface [3,4], which are described by Equations 1-3.

$$\Delta P_c = \frac{2\sigma\cos\theta}{r_c} \quad \text{Eq. 1}$$

$$\Delta P_g = \rho g h \quad \text{Eq. 2}$$

$$h = \frac{2\sigma\cos\theta}{\rho g r_c} \quad \text{Eq. 3}$$

In a given gravitational environment, the liquid column height (h) is related to geometric properties as contact angle (θ) and effective pore radius (r_c) as well as fluid properties surface tension (σ) and density (ρ).

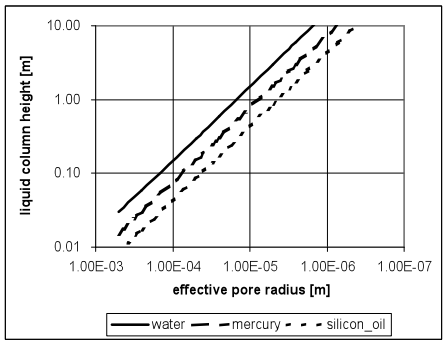

Figure 2: Liquid column height for different fluids (fluid properties from table 1)

		Water	*mercury*	*silicon oil*
σ	[N/m]	73E-3	500E-3	16E-3
ρ	[kg/m^3]	0.998E+3	13.5E+3	0.76E+3
σ/ρ	[Nm^2/kg]	73.1E-6	37.0E-6	21.1E-6

Table 1: Fluid properties used for calculations (P=1 atm, T=293K)

Figure 2 gives the theoretical liquid column height for different fluids and wick effective pore radius from Equation 3. From Figure 2 it can be observed that the rising meniscus method can be impractical for wick structures with micro- or nano-sized effective pore radius, as column heights can easily exceed practical laboratory dimensions.

Adkins et al. [6,7] describe the method of using a bubble point test for measurement of the largest pore size in the sample. In this bubble point test, the wick structure is saturated with a fluid and gas is forced through the wick by applying a pressure difference across the sample. If one side of the sample is completely submerged, this pressure can be identified by the formation of vapor bubbles, giving the test its name. The effective pore radius is inversely proportional to the required pressure difference, which can be derived from Equation 4.

$$r_c = \frac{2\sigma\cos\theta}{\Delta P_c} \quad \text{Eq. 4}$$

The bubble point test idealizes the pore as a circular hole and measures the largest pore flow path. This technique is only able to characterize the minimum capillary performance of a wick structure. Due to variation in pore sizes, the maximum capillary performance can be substantially different [1].

This study describes the method of characterizing the capillary performance of micro- and nano-scale wick structures using a bubble point test setup. Steps described include validation of measurement technique, preparation of micro- and nano-wick samples for testing and measurement results. In addition, a novel visualization method is presented for capillary flow in porous structures.

MEASUREMENT OF CAPILLARY PERFORMANCE

The apparatus chosen for performing the bubble point testing is a PMI bubble point tester. This apparatus allows a sample to be placed between two O-rings. Subsequently the sample is wetted with a testing fluid (see Figure 3).

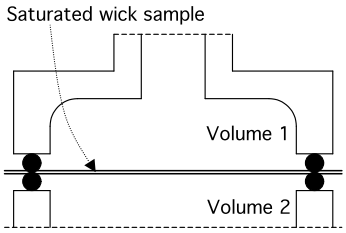

Figure 3: Sketch of bubble point test setup

The pressure of the volume on one side of the sample is increased in small steps. The point at which air passes through the sample can be identified by the inability to increase the pressure in volume 1 any further. The pressure difference across the sample at this point is the bubble point pressure and can be related to the largest pore diameter using Equation 4.

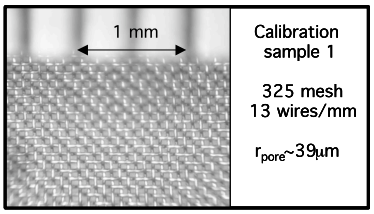

Figure 5: Image of 325 mesh

A structure with known pore diameter is required to effectively validate the described measurement system. For this validation test, wire meshes with known structure were acquired and tested using the bubble point machine. Samples of 325 and 150 size woven stainless steel mesh were prepared for calibration (Figure 5). The effective pore radius of pores in such a mesh is estimated using the screen mesh number (N) and Equation 5 given by Chi[8].

$$r_c \approx 1/2N \quad \text{Eq. 5}$$

Using Equation 5 the 325 mesh and 150 mesh the effective pore radii are estimated to be 39.1 and 84.7 µm

NSTI-Nanotech 2009, www.nsti.org, ISBN 978-1-4398-1784-1 Vol. 3, 2009

respectively. A parameter required for the evaluation of the measured effective pore radius is the contact angle between the sample material and the testing fluid. Contact angles between fluids and wire meshes were measured and data was corrected using the measured contact angles.

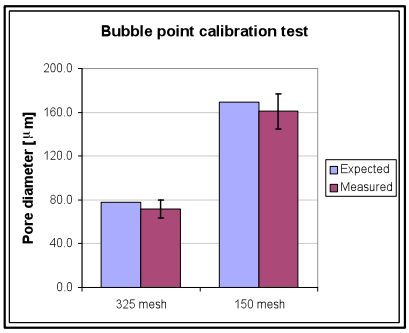

Figure 7: Wire mesh bubble point validation test results, error bars set at one standard deviation

The fluids used were distilled water and isopropyl alcohol, and tests were repeated at least ten times with different samples of the same mesh size. It is expected that there is some error in the calculated effective pore radius due to the transition from square pore geometry to a simplified effective radius. In addition, the fact that the mesh is woven adds three-dimensional offset to one half of the squares sides. Nevertheless, the test data shown in Figure 7 fell within one standard deviation of the calculated estimate.

CAPILLARY PERFORMANCE RESULTS

Iverson[3] points out some of the challenges in characterizing the mean effective pore radius of porous samples using the bubble point method. Due to the non-homogenous nature of porous structures, the bubble point method is expected only to give information on the minimum capillary performance of a structure.

In order to test samples of porous wick structures with small effective pore radii, a method was developed for preparing the samples for the bubble point test. A challenge that had to be addressed is that porous structures with micro- or nano-sized pores (Figure 8, left) can be extremely fragile and therefore cannot be clamped into the test fixture as sketched in Figure 3. In addition, the bubble point test method requires the structure to have sufficient strength to withstand the pressure difference across the sample without fracturing.

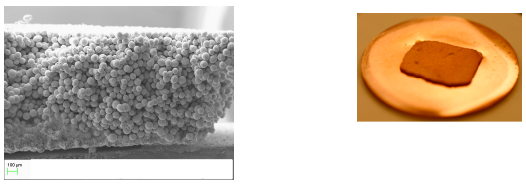

Figure 8: SEM image of wick structure (left) and prepared sample of copper wick on copper adapter (right)

This challenge is often addressed by use of an adapter plate with a smaller diameter. The sum of the distributed load force on the sample scales inversely with area and therefore inversely with the diameter squared. By reducing the opening diameter, the stresses on the sample can be greatly reduced. The porous structure then sits as a "bridge" across this smaller diameter opening. A four-step procedure is presented to prepare the sample on the adapter disc. First, a small center hole is drilled in the disc by laser. The diameter of this hole is chosen to be at least one order of magnitude greater than the expected largest pore radius of the wick sample. The center hole is then filled with wax filler. The wax plug facilitates the placement of the wick structure on the disc and prevents wick particles from entering the hole. After the wick is placed on the disc, the disc and wick are sintered together to eliminate leakage paths between the wick and disc. During this process, the filler melts and the sample is ready for testing (Figure 8, right).

An advantage of this method is that if the diameter of the clamp is greater than the wick sample, the disc will be clamped between the o-rings while the sample remains uncompressed. One must however note that this method provides only a single point measurement over the wick "bridge". If large variations in performance are expected, it is possible to use multiple holes in the disc for characterization. A porous wick sample was prepared using copper particles of 75 μm mean diameter (Figure 8). SEM images of the sample showed that a small variation exists in the diameters of the particles (Figure 8). The prepared wick sample was sintered to a larger support disc structure using the described method. The bubble point test was performed using isopropyl alcohol and repeated six times (Figure 9).

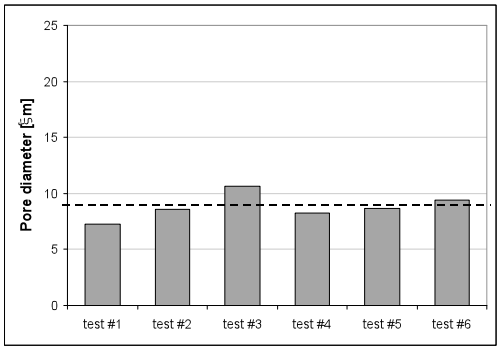

Figure 9: Bubble point test measurement results for copper wick sample

The mean measurement pore diameter of the sample was found to be 8.8 μm. A modest deviation in measurement results is observed. A mean pore diameter of 8.8 μm for a sample with particle diameter of 75 μm is significantly smaller than initially expected based on work by Chi[8]. Taken into account that factors such as particle shape, necking between particles and porosity all potentially affect the capillary performance of porous structures, a deviation from the simplified correlation by Chi[8] is not unexpected.

FLOW VISUALIZATION USING FLUORESCENT DYES

Flow visualization experiments were conducted to measure the capillary performance of the copper wicks. A 1% solution of IFWB-C7 fluorescent dye (Risk Reactor Inc.) dissolved in methanol was used for imaging. An ultraviolet lamp was used as the light source in combination with a regular video camera. A UV filter was attached in front of the camera lens to block the incident light and image only the fluorescent light emitted by the dye. The wick was held vertical and lowered into a beaker containing the fluorescent dye solution. Figure 10 shows images of the dye front as it rises along the wick.

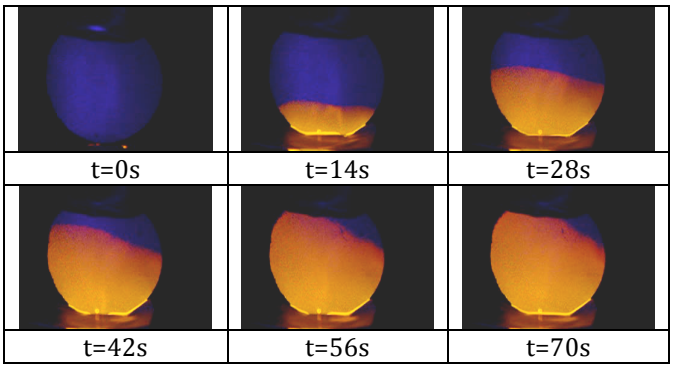

Figure 10: Visualization of wick saturation in copper sintered wick of 75 µm using fluorescent dye (circular wick sample in vertical orientation)

From Figure 10 it can be observed that the liquid column sees a very large acceleration at $t = 0s$ and decelerates over time. Under first principle, this agrees with the standard differential equation for capillary rise where the liquid column acceleration is inversely proportional to the liquid column height. After $t = 30s$, the liquid level stabilizes and the rise becomes more irregular. From Figure 10 it can be observed up to $t = 30s$ the global rise is relatively uniform across the sample. After this point, the left side of the wick sees a more rapid rise than the right side of the sample. This local deviation in rise could be caused by non-homogenous porosity or necking structure or particle diameter.

The presented visualization technique provides a novel method of analyzing wick performance as it tracks liquid rise over time providing information on both capillary and permeability performance of the sample.

CONCLUSIONS

Experimental validation of capillary performance of wick structures is crucial in the development of high performance heat pipes. A discussion is presented in which the challenges of measuring such performance for wicks with micro- to nano-sized wick structures is highlighted. The advantages and disadvantages of using a bubble point test method for evaluation of such performance are presented. A disadvantage of the bubble point method is that it gives a minimal capillary performance. If the sample has a large variation in pore sizes, this might not be a good representation. However, if the spread in pore size is reasonable, the bubble point method proves to be a fast and simple method to get an initial estimate for sample performance.

Test data is presented in which the bubble point setup is validated using fine wire mesh screens. It was found that although there was a minor variation in measured effective pore radius, the data falls within one standard deviation of expected calculated values.

A four-step method is presented for preparing a wick sample for the bubble point method using a larger disc with a center hole. The center hole is initially filled with wax filler, which is baked off during the process of sintering the wick structure to the disc. This method provides a process for sample preparation where the wick structure is minimally loaded. If large variations in capillary performance across a single sample are expected, multiple holes can be made into the disc.

A copper wick sample is presented and characterization results are presented. The measured mean pore diameter was found to be significantly smaller than suggest by work by Chi. It is expected that factors such as particle shape, necking between particles and porosity affect the mean pore diameter of a sample.

A novel method for saturation visualization is presented in which a sample is saturated using a fluid with a fluorescent dye. An ultraviolet light source and a camera with UV-filter are used to track the fluorescent dye front through the sample. Using a post-processing algorithm, the dye front rise as a function of time was established. The wick visualization technique is found to be a valuable method for obtaining information on the wick global and local capillary and permeability performance.

ACKNOWLEDGMENTS

This paper is based upon work supported by DARPA under SSC SD Contract No. N66001-08-C-2008. Any opinions, findings and conclusions or recommendations expressed in this material are those of the author(s) and do not necessarily reflect the views of the SSC San Diego.

REFERENCES

1. http://www.darpa.mil/mto/programs/tgp/index.html
2. Peterson G.P. 1994, An Introduction to Heat Pipes
3. Iverson, B.D et.al. 2007 *Journal of Thermophysics and Heat Transfer,* Vol. 21, No. 2, 2007
4. Faghri, A, 1995, Heat Pipe Science and Technology
5. Semenic, T, et.al. 2008, *Journal of Heat Transfer,* Vol. 130, Issue 2, 022602,
6. Adkins, D.R., Moss, T., 1990, *Solar Engineering*
7. Adkins, D. R. etal *28th Intersociety Energy Conversion Engineering Conference,* Vol. 2, 1993, pp. 911–917.
8. Chi, S. W., 1976, Heat Pipe Theory and Practice,